

Numerical investigation on the surface crack growth in FRP-reinforced steel plates subjected to tension

Li, Zongchen; Jiang, Xiaoli; Hopman, Hans; Zhu, Ling; Liu, Zhiping

DOI

[10.1016/j.tafmec.2020.102659](https://doi.org/10.1016/j.tafmec.2020.102659)

Publication date

2020

Document Version

Final published version

Published in

Theoretical and Applied Fracture Mechanics

Citation (APA)

Li, Z., Jiang, X., Hopman, H., Zhu, L., & Liu, Z. (2020). Numerical investigation on the surface crack growth in FRP-reinforced steel plates subjected to tension. *Theoretical and Applied Fracture Mechanics*, 108, Article 102659. <https://doi.org/10.1016/j.tafmec.2020.102659>

Important note

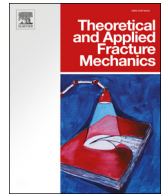
To cite this publication, please use the final published version (if applicable). Please check the document version above.

Copyright

Other than for strictly personal use, it is not permitted to download, forward or distribute the text or part of it, without the consent of the author(s) and/or copyright holder(s), unless the work is under an open content license such as Creative Commons.

Takedown policy

Please contact us and provide details if you believe this document breaches copyrights. We will remove access to the work immediately and investigate your claim.



Numerical investigation on the surface crack growth in FRP-reinforced steel plates subjected to tension

Zongchen Li^{a,*}, Xiaoli Jiang^a, Hans Hopman^a, Ling Zhu^b, Zhiping Liu^c

^a Department of Maritime and Transport Technology, Delft University of Technology, 2628 CD Delft, the Netherlands

^b Departments of Naval Architecture, Ocean and Structural Engineering, School of Transportation, Wuhan University of Technology, 430063 Wuhan, PR China

^c Port Logistic Technology and Equipment Research Centre of Ministry of Education, 430063 Wuhan, PR China

ARTICLE INFO

Keywords:

Surface crack
Finite element method
Fibre-reinforced polymer
Stress intensity factor
Structural integrity

ABSTRACT

In this paper, we analyse the surface crack growth in the Fibre-Reinforced Polymer (FRP) reinforced steel plates subjected to tension by means of the finite element (FE) method. Following the experimental study, a three-dimensional FE model is developed to evaluate the Stress Intensity Factor (SIF) of the surface crack, and the crack growth rate is calculated by using the Paris' law. Then the FE model is validated by the experimental results. Afterwards, on account of the validated FE model, a parametric study is developed in order to guide the optimization design of FRP reinforcement accounting for different reinforcing schemes and multiple influential parameters. The results indicate that the single-side FRP reinforcement on the cracked surface is the most efficient method, owing to the generated out-of-plane bending moment. In addition, the optimum bond length and number of layers are indicated. Besides, surface crack growth is sensitive to the influential parameters including aspect ratio of the surface crack and crack dimension, while less sensitive to the Carbon-FRP (CFRP) tensile modulus, and the adhesive thickness. The analysis is of instructive value to facilitate the application of FRP reinforcement on the surface cracked metallic structure repairing domain.

1. Introduction

The surface crack is a common defect in the metallic structures, which can be initiated from surface damages, fretting corrosion, or corrosion pitting [1–3]. In practical situations, surface cracks might continually propagate under cyclic loads, resulting in serious threat to the structural integrity in the fields of aerospace engineering [4], pressure vessels and nuclear reactors [5,6], as well as transportation pipelines [7,8].

Preventing surface crack growth is of great importance. In recent years, the Fibre-Reinforced Polymer (FRP) reinforcement has been applied as a well-recognised alternative of the traditional fatigue crack repairing methods such as welding, drilling stop holes, or bolting [9]. It has been highly valued for repairing cracked metallic structures, owing to its outstanding advantages in terms of efficiency, cost-effective, no secondary damage and ease of installation [10–12]. To date, researchers have conducted various investigations of using FRP to repair cracked metallic structures, majorly on repairing through-thickness cracks [13–16]. However, the investigation of FRP reinforcement on surface cracked metallic structures is seriously insufficient. Although the FRP reinforcement on internal surface cracked pipes has been

studied recently [17,18], the FRP patches in those cases did not contact with the surface crack, hence the interaction between the FRP patch and the surface crack is still unclear. Besides, the investigations on repairing through-thickness cracks using FRP is not directly referable, owing to the different crack profiles and failure modes. Therefore, the investigations of the FRP reinforcement on surface cracked metallic structures need special attention.

In the separate study by using an experimental investigation, the effectiveness and possible failure modes of using FRP to reinforce the surface cracked steel plates subjected to cyclic tension have been identified [18]. The results concluded that the FRP reinforcement had significantly decreased the fatigue crack growth rate (FCGR) of the surface cracks, and the interfacial failures did not occurred on the majority of the specimens. While further and in-depth investigations are still in a great demand to reveal the mechanism of the FRP reinforcement on surface cracked metallic structures, in order to facilitate the development of FRP reinforcement.

Given that, we conduct a finite element (FE) analysis on surface cracked steel plates reinforced with the FRP. The main objective of this paper is to analyse the crack growth behaviour reinforced with FRP. In Section 2, a three-dimensional FE model is developed to evaluate the

* Corresponding author.

E-mail address: z.li-8@tudelft.nl (Z. Li).

Nomenclature

| | |
|---------|--|
| a | crack depth of surface cracks |
| a/c | aspect ratio of surface cracks |
| b | plate width |
| C | Paris' law constant |
| C_a | Paris' law constant for the deepest point |
| C_c | Paris' law constant for the surface point |
| c | half crack length of surface cracks |
| da/dN | crack growth rate along the depth direction |
| dc/dN | crack growth rate along the length direction |
| E_i | elastic modulus |

| | |
|-----------------|--|
| G_{ij} | shear modulus |
| Q | correction factor of the surface crack |
| R | stress ratio |
| m | Paris' law constant |
| ν | Poisson's ratio |
| T | tensile strength |
| t | thickness of the plate |
| K_I | the SIF along the surface crack front |
| ΔK_{Ia} | the range of SIF of the deepest point of the surface crack |
| ΔK_{Ic} | the range of SIF of the surface point of the surface crack |
| σ_t | tension normal stress |
| φ | the eccentric angle of the surface crack |

Stress Intensity Factor (SIF) of the surface cracks in steel plates reinforced with FRP. In Section 3, the FE model is validated by conducting an experimental investigation. Then based on the validated FE model, in Section 4, we conduct a parametric study to identify the optimum reinforcement schemes and the key influential parameters of the FRP reinforcement in order to guide an optimization design. Finally the conclusions are drawn in Section 5.

2. Experimental study

In this section, the experimental study on surface cracked steel plates reinforced with FRP subjected to cyclic tension is conducted. In total, eight groups of 23 specimens were conducted, where six groups of 18 specimens were conducted for the validation purpose, and the rest of the specimens were for the parametric study in Section 4. Note that more detailed information and analysis of the experiments can be referred to our previous study [19].

2.1. Materials properties

The sketch diagram of FRP reinforced surface cracked plate is shown in Fig. 1. The specimens contains four different materials: the steel substrate, Glass-FRP (GFRP), Carbon-FRP (CFRP), and adhesive. The material properties of the GFRP, CFRP and adhesive are listed in Tables 1–3 respectively. Stainless steel of 907A for subsea scenarios conforming to GJB 6055–2007 code [20] has been used as the steel substrate, which has a yield strength of 390 MPa, and tensile strength of 530 MPa. The CFRP laminate used the T700S series unidirectional fabric in order to achieve an efficient reinforcement. While the GFRP laminates applied the E-fibre weave fabric for the purpose of eliminating the potential of galvanic corrosion between the steel substrate and the CFRP laminates. Note that no special consideration has been made in regard to the mechanical properties of GFRP. The adhesive adopted the resin epoxy. The material properties of steel, FRP and

adhesive are all provided by each manufacturer.

2.2. Specimen preparation and configuration

Semi-elliptical notches were first manufactured by means of the Micro-Electric Discharging machining (Micro-EDM). This method can achieve user designed notch profiles, as well as avoiding thermal residual stress [21]. The manual notches are located in the middle of each steel plate, orientating perpendicular to the length direction of the steel plate. However, the semi-elliptical shaped notches were not yet fatigue cracks. Therefore, a pre-cracking procedure was conducted on each steel plate to initiate the semi-elliptical fatigue crack that let the surface crack propagate at least 1.0 mm [22].

Afterwards, the surface cracked steel plates were reinforced with the FRP patch. As is acknowledged, a properly prepared surface of the steel substrate is of great important to achieve a success FRP reinforcement. In this study, solvent cleaning and sanding were adopted for the surface preparation. Then the steel plates were reinforced with the FRP patch by hand lay-up technique. After that, the FRP laminates were compressed by a large mass to squeeze the redundant resin epoxy and eliminate the bubbles in the interlaminations, as well as guarantee that the FRP patches were tightly bonded on the steel plate. Finally the specimens were placed under ambient temperature of one week to ensure for fully solidification. The details of the configuration of the experimental specimens, such as initiation crack sizes, sizes of the steel specimens, and the detailed reinforcement schemes, can be referred to Ref. [19].

The steel plate is 400 mm long, 60 mm wide and 12.3 mm thick. The surface crack is located in the middle of the steel plate, orienting perpendicular to the length direction. The FRP patch, which contains one layer of GFRP and four layers of CFRP, is bonded on the steel plate. The thickness of each layer of GFRP and CFRP laminate are 0.35 mm. Each FRP reinforced specimen applies one layer of GFRP as the first layer, and several layers of CFRP laminate on top of that, as shown in Fig. 2. In

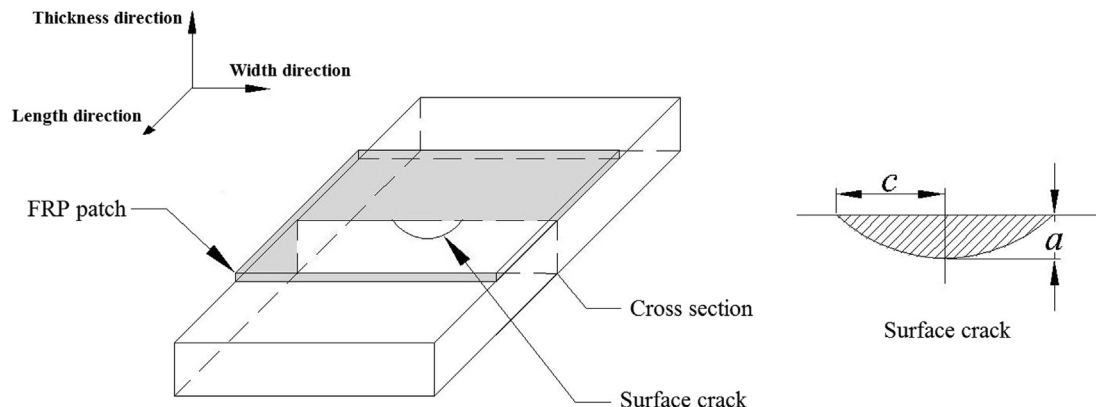


Fig. 1. The sketch diagram of single-FRP reinforced surface cracked plate on the cracked surface.

Table 1
Material properties of GFRP material.

| E_1 (Pa) | E_2 (Pa) | T (Pa) | G_{13} (Pa) | G_{23} (Pa) | Nu |
|------------------|------------------|-------------------|-------------------|-------------------|------|
| 72×10^9 | 72×10^9 | 1.1×10^9 | 4.7×10^9 | 3.5×10^9 | 0.33 |

Note: E_1 and E_2 are the elastic modulus along length and width direction; T is the tensile strength; G_{13} and G_{23} are the shear modulus; Nu is the Passion's ratio.

Table 2
Material properties of the CFRP material.

| E_1 (Pa) | E_2 (Pa) | T (Pa) | G_{13} (Pa) | G_{23} (Pa) | Nu |
|-------------------|------------------|-------------------|-------------------|-------------------|------|
| 230×10^9 | 25×10^9 | 4.9×10^9 | 5.5×10^9 | 3.9×10^9 | 0.3 |

Table 3
Material properties of the resin epoxy.

| E (Pa) | T (Pa) | G (Pa) | Nu |
|-------------------|------------------|-------------------|------|
| 2.8×10^9 | 70×10^6 | 1.4×10^9 | 0.35 |

total, nine groups of 23 specimens were prepared. Each group has three repetitive specimens, as listed in Table 4. Group 1, 2, and 3 are three controlling group of three different groups of initial surface crack sizes without FRP reinforcement. Group 4 used FRP to reinforce the reversed side of the cracked surface, while Group 5, 6, and 7 used FRP to reinforce the cracked surface with different crack sizes. Most groups have three repetitive specimens except Group 8 & 9 which have only one specimen each. The specimens were named after their groups, reinforcement schemes, and repetitive number. For example, the specimen 'SE-1-R(1)', 'S' means steel plate, 'E' represents reinforcing the steel plate on the cracked surface, 'R' means reinforcement, the first '1' stands for the first type of notch, and the second '1' means the No. of the repetitive specimen.

2.3. Test set-up

A 250 kN MTS Hydraulic Actuator was used to conduct the fatigue test. All the specimens were clamped by a pair of hydraulic clamps, positioned horizontally on the fatigue machine, as shown in Fig. 3. The fatigue tests followed the code of ASTM E647 [22]. All tests were conducted at room temperature under load control condition. Constant amplitude sinusoidal cyclic loading were applied on the specimens. The loading frequency was set to be 12.0 Hz, and the load ratio $R = 0.1$. The crack growth process was recorded by beach marking technique.

The method is to change R from 0.1 to 0.5 for 5000 cycles between every 10,000 cycles, while the load amplitude remained unchanged. Eventually, each specimen fractured along the crack plane and triggered the displacement limiter to end the test.

A strain gauges matrix is installed on the external layer of CFRP laminate of each specimen, as shown in Fig. 3b. The matrix can cover $25.0 \text{ mm} \times 4.0 \text{ mm}$ around the central cracked area. Then the gauges are connected to the dynamic strain indicator TMR™-300, which will detect the crack-debonding during the fatigue. The reason when crack-induced debonding occurs, the strain on the external layer of the CFRP laminate will drop dramatically, because there is no transfer of shear stress in the debonding region [23].

2.4. Test phenomenon and results

During the fatigue test, the majority of the specimens did not encounter with the failures of FRP reinforcement. While four out 14 FRP reinforced test specimens failed owing to the interfacial debonding, i.e., edge debonding and crack-induced debonding, which are SE-1-R(1), SE-1-R(2), SE-2-R(3), and SE-1-R6(1). The edge debonding failures were observed by naked eyes (see in Fig. 4), while the crack-induced debonding failures were detected by the strain gauges around the cracked areas. The major reason of edge debonding were owing to the free-edge effect which was induced by the mismatch of the elastic properties of the materials at the edges [24,25]. Edge debonding were occurred on several specimens at the very beginning of the test, hence the imperfect bonding condition by the hand lay-up technique might be a fuse of the failures as well. As a result, these failed specimens will not be used to validate the FE models. The surface crack growth results of the specimens with perfect bonding condition will be presented along with the FE results for validation purpose in Section 3. The detail of the failure modes and experimental results are analysed and discussed in Ref. [19].

The crack growth behaviour was recorded by the beach marking technique using an electronic reading microscope, as shown in Fig. 5. The cycle index between each two adjacent beach marks is 10,000. The figures clearly demonstrate that surface cracks continually propagated as a semi-elliptical shape until the crack penetrated the pipe wall. The results of crack depth and length, corresponding to the cycle-index are listed in Ref. [19].

3. Finite element analysis

The FE method is an efficient method to evaluate the SIF of surface cracks in metallic structures reinforced with composite patches [8]. In this section, a three-dimensional FE model is developed to calculate the SIF of the surface crack in FRP reinforced steel plates. The FE model is developed using the commercial code ANSYS workbench 19 [26]. The

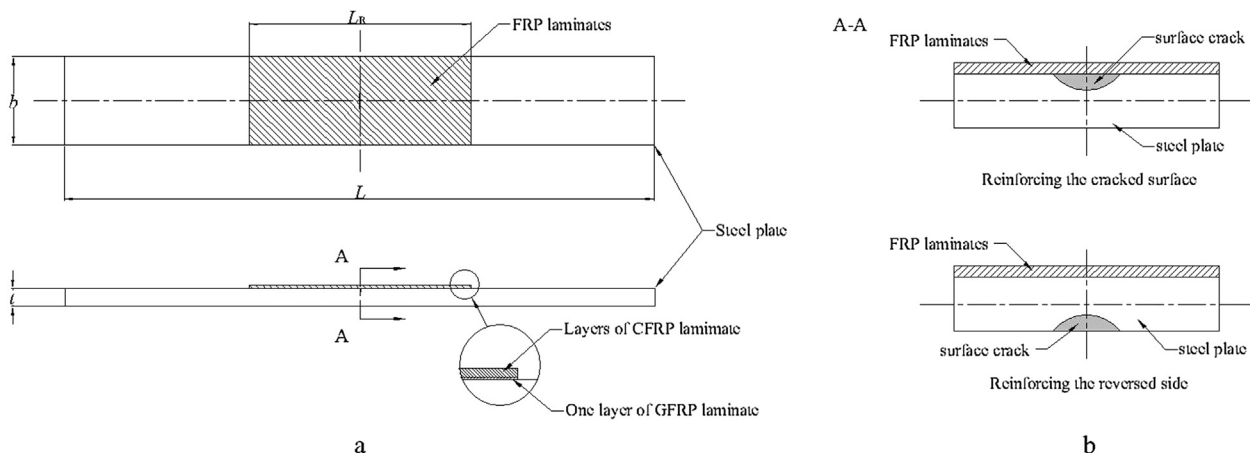


Fig. 2. The configuration of specimens: a) a FRP reinforced steel plate; b) the location of a surface crack in a steel plate.

Table 4
Specimens' configurations and reinforcement details.

| Group | Specimen | Notch category | b (mm) | t (mm) | a_0 (mm) | c_0 (mm) | The reinforced surface | No. of CFRP layer |
|-------|------------|----------------|----------|----------|------------|------------|------------------------|-------------------|
| 1 | S-1(1) | 1 | 59.86 | 12.39 | 1.90 | 5.00 | / | / |
| | S-1(2) | 1 | 59.95 | 12.33 | 1.86 | 5.00 | / | / |
| | S-1(3) | 1 | 59.86 | 12.36 | 1.92 | 4.98 | / | / |
| 2 | S-2(1) | 2 | 59.87 | 12.32 | 1.96 | 3.15 | / | / |
| | S-2(2) | 2 | 59.43 | 12.36 | 1.90 | 3.15 | / | / |
| | S-2(3) | 2 | 59.87 | 12.36 | 1.96 | 3.14 | / | / |
| 3 | S-3(1) | 3 | 59.80 | 12.39 | 3.98 | 4.00 | / | / |
| | S-3(2) | 3 | 59.78 | 12.43 | 3.96 | 3.98 | / | / |
| | S-3(3) | 3 | 59.69 | 12.45 | 3.95 | 3.98 | / | / |
| 4 | SI-1-R(1) | 1 | 59.45 | 12.30 | 1.96 | 5.00 | The reversed side | 4 |
| | SI-1-R(2) | 1 | 59.92 | 12.28 | 1.86 | 4.95 | The reversed side | 4 |
| | SI-1-R(3) | 1 | 59.85 | 12.34 | 1.86 | 4.95 | The reversed side | 4 |
| 5 | SE-1-R(1) | 1 | 59.79 | 12.41 | 1.90 | 5.02 | The cracked surface | 4 |
| | SE-1-R(2) | 1 | 59.67 | 12.34 | 1.90 | 4.86 | The cracked surface | 4 |
| | SE-1-R(3) | 1 | 60.02 | 12.36 | 1.88 | 4.99 | The cracked surface | 4 |
| 6 | SE-2-R(1) | 2 | 60.01 | 12.41 | 1.91 | 3.10 | The cracked surface | 4 |
| | SE-2-R(2) | 2 | 59.52 | 12.42 | 1.86 | 3.13 | The cracked surface | 4 |
| | SE-2-R(3) | 2 | 59.96 | 12.43 | 1.90 | 3.08 | The cracked surface | 4 |
| 7 | SE-3-R(1) | 3 | 59.95 | 12.47 | 3.90 | 3.89 | The cracked surface | 4 |
| | SE-3-R(2) | 3 | 60.13 | 12.38 | 3.90 | 3.94 | The cracked surface | 4 |
| | SE-3-R(3) | 3 | 59.84 | 12.22 | 3.89 | 3.94 | The cracked surface | 4 |
| 8 | SE-1-R2(1) | 1 | 60.07 | 12.30 | 1.95 | 4.95 | The cracked surface | 2 |
| 9 | SE-1-R6(1) | 1 | 60.04 | 12.40 | 1.91 | 5.00 | The cracked surface | 6 |

Note: The parameters, i.e., b , t , a_0 , c_0 are measured based on each specimens, each of which is the weighted average of three measurement locations.

materials and size of the models are identical to the experimental specimens in Section 2.

3.1. Configuration of the FE models

The materials, dimensions and initial crack sizes of the FE models conform to the tests. Different reinforcing schemes are applied on the FE models: (1) single-side reinforcement on the cracked surface; (2)

single-side reinforcement on the reversed side of the cracked surface; (3) double-side reinforcement on both sides. The principle direction of the unidirectional CFRP is parallel to the force direction. The FRP patch is located in the middle of the specimens, which is 150 mm long, 60 mm wide. The thickness of the adhesive, GFRP laminate, and each layer of CFRP laminate are 0.1 mm, 0.35 mm, and 0.35 mm respectively. Therefore, the overall patch thickness is 1.85 mm, which is identical to the thickness of the test specimens. Hence, the FE model is developed

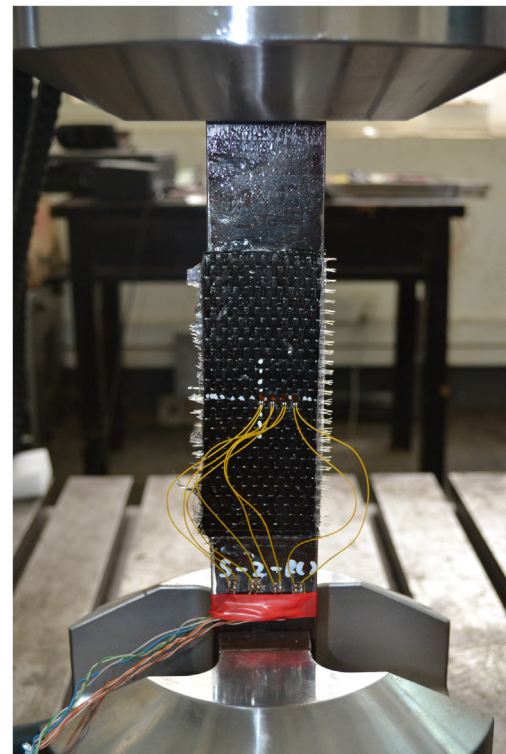
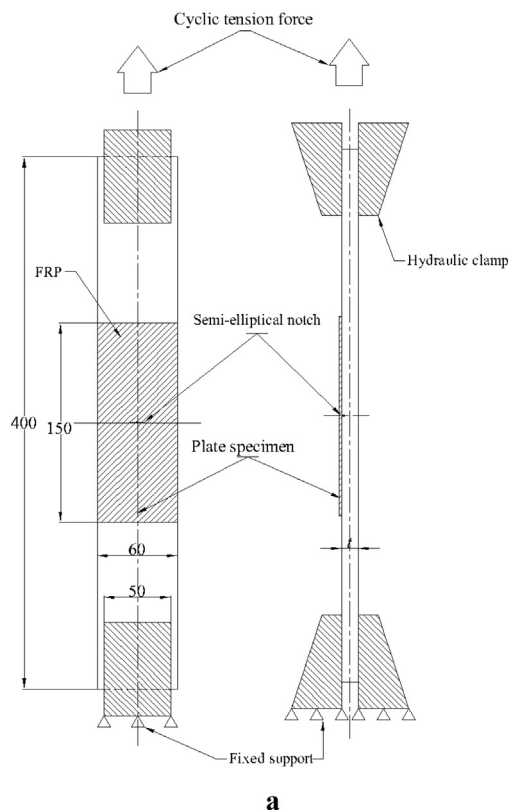


Fig. 3. Specimen installation: a) the schematic; b) the actual specimen installation.

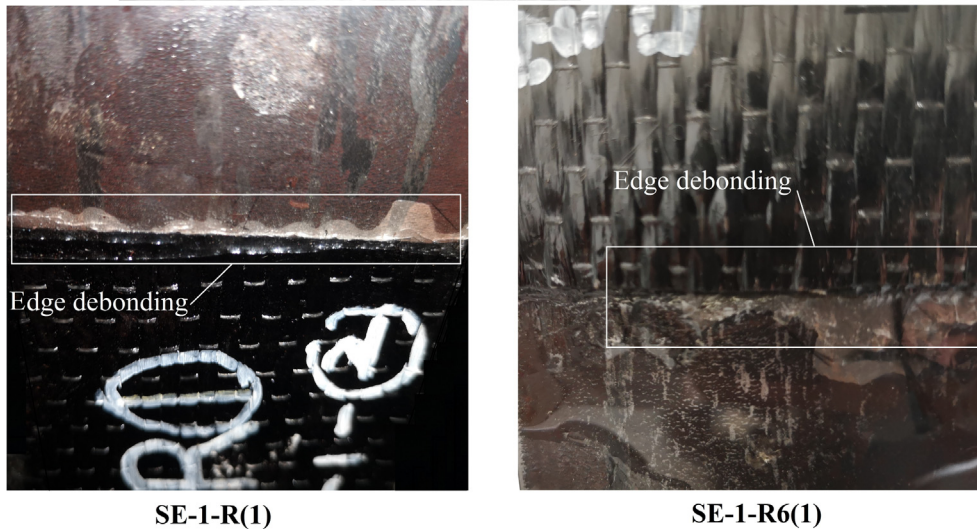


Fig. 4. Edge debonding occurred during the fatigue test.

based on the actual situation in terms of the overall patch thickness and the fact that no delamination failures within the FRP laminates occurred during the fatigue test – different layers of FRP laminates are modelled as a whole, by merging the bodies together while remain their own material properties and fibre directions. Table 5 lists the configurations of the FE models.

3.2. FE modelling strategy

The modelling strategy (e.g., element type, meshing method, element size, contours around the crack front and their divisions) has been discussed through the sensitivity analysis in previous studies to ascertain that the FE model is able to rationally predict the SIF [18]. The FE model adopts 20-node solid element ‘solid 186’. Two different meshing methods are applied to the steel plate: the middle part where the crack is located adopts the tetrahedral meshing method; while the other two parts apply the sweep meshing method with hexahedral element. The sweep method is applied for the FRP laminates as well. To ensure a robust and accurate evaluation, a 1.0 mm body element size is used for the area around the surface crack and the adhesive layer, while 5.0 mm edge size is used for the rest parts of the steel plate, as well as the FRP patch, as shown in Fig. 6.

The semi-elliptical surface crack is modelled by the *Semi-elliptical Crack* module in ANSYS workbench 19 [26]. Six concentric contours with eight divisions of each are modelled around the surface crack front, as shown in Fig. 7a. Then the surface crack is meshed using hexahedra dominant method, as shown in Fig. 7b. The size of the external contour is 1.0 mm, thus the element size around the crack front is controlled as less than 0.2 mm.

Since the FRP laminates are modelled as a whole, setting the contact condition between the adjacent FRP layers is not necessary. While bond

condition is set at the interface between the steel substrate and the adhesive layer, and at the interface between the adhesive layer and the GFRP laminate. Then the model is set to be subjected to tension – one side is fixed supported, while tensile load is applied on the other side. The amplitude of the tensile load is 168.48 kN (equals to 228.3 MPa on the load bearing surface), which is about 60% of the yield strength of the steel material. Finally, the SIF along the crack front is calculated by means of the contour integral method.

3.3. FE results

In this sub-section, the FE results of the global and local stress distribution, as well the SIF along the surface crack front are presented. The results demonstrate the effectiveness of the FRP reinforcement on the decreasing of stress distribution and the SIF along the surface crack front preliminarily, while further validation of the FE results will be presented in Section 3.

3.3.1. Global and local stress distribution in the steel plate

The global equivalent stress distribution on the steel plate of ‘S-1’ and ‘SE-1-R’ models are shown in Fig. 8. It illustrates that under the FRP reinforcement, the stress decreases dramatically, especially in the area covered by the FRP. The maximum stress has dropped from 2877.6 MPa to 1240.5 MPa, of 56.89%. Fig. 9 indicates that the stress concentrates around the surface cracked area where the maximum point located at the surface point. Owing to the FRP reinforcement, the stress concentration zone around the surface crack, represented as the butterfly zone, becomes smaller.

3.3.2. SIF along the surface crack front

Further on, the results of the SIF along the surface crack front of



Fig. 5. Beach marks on the cross-section of the steel plate specimens.

Table 5
The configurations of the FE models.

| FE model | Initial crack size (mm) | | Reinforcement scheme | Reinforced surface | No. of CFRP layer |
|------------|-------------------------|-----------------------|---------------------------|--------------------|-------------------|
| | Crack depth a | Half crack length c | | | |
| S-1 FE | 5.24 | 6.50 | no reinforcement | / | / |
| S-2 FE | 4.48 | 4.70 | no reinforcement | / | / |
| S-3 FE | 5.40 | 5.78 | no reinforcement | / | / |
| SE-1-R FE | 6.25 | 6.33 | single-side reinforcement | cracked surface | 4 |
| SE-2-R FE | 4.48 | 4.68 | single-side reinforcement | cracked surface | 4 |
| SE-3-R FE | 6.11 | 6.40 | single-side reinforcement | cracked surface | 4 |
| SI-1-R FE | 5.66 | 6.54 | single-side reinforcement | reverse surface | 4 |
| SE-2-RD FE | 4.48 | 4.68 | double-side reinforcement | double sides | 8 |

both the un-reinforced and FRP reinforced specimens are shown in Fig. 10. Fig. 10a show the surface crack configuration and a point P at the crack front, which can be identified by the eccentric angle φ . The SIF of different points along the crack front are shown in Fig. 10b. The SIFs along the crack front of a small crack of $a = 6.25$ mm, $c = 6.33$ mm, and a large crack of $a = 9.98$ mm and $c = 10.93$ mm are investigated. Note that these two crack sizes are derived from the FE model of SE-1-R from the start and the later stage respectively. It clearly shows that the FRP reinforcement decreases the SIF at both stages, but the effectiveness is different: for the small crack, the SIFs of the surface crack depth point and the deepest point decrease 10.20% and 4.93% respectively; while for the large crack, the SIFs of the surface crack depth point and the deepest point decrease 12.46% and 2.24% respectively. Hence it indicated that: (1) FRP reinforcement is more effective on the surface point than on the deepest point, which might be owing to the crack-bridging effect; (2) along with the crack propagation, the effectiveness of the FRP reinforcement increases on the surface point while decreases on the deepest point.

3.3.3. Stress distribution in the adhesive layer

The results of the equivalent stress distribution in the adhesive layer adjacent to the steel substrate with a small crack of $a = 6.25$ mm, $c = 6.33$ mm, and a large crack of $a = 9.98$ mm and $c = 10.93$ mm are shown in Fig. 11. It demonstrates that the stress concentration mainly occurs at two areas – the edge area and the central area. Besides, the stress concentration with a large surface crack is more serious than with a small surface crack in terms of the area and maximum stress value. Therefore, along with the surface crack growth, the local stress concentration at the central area might be a potential safety hazard of the crack-induced debonding respectively. In addition, stress concentration was also occurred at the edge of the reinforcement. Besides the free-edge effect, the local stress concentration might contribute to the edge debonding as well.

3.4. Experimental validation

In this sub-section, the experimental results of surface crack growth and FE results are compared and analysed. First, the Paris' constants are calibrated on account of the experimental results. Then, the FE model is validated by the experimental results.

3.4.1. Paris' constant calibration

The SIFs of the surface crack in the models without FRP reinforcement are calculated by means of Newman-Raju's equation [4], which is

$$K_I = \sigma_t \cdot \sqrt{\pi \frac{a}{Q}} \cdot F\left(\frac{a}{t}, \frac{a}{c}, \frac{c}{b}, \varphi\right), \quad (1)$$

where σ_t is the tension normal stress, Q is an approximation factor, $F(a/t, a/c, c/b, \varphi)$ is the boundary correction factor. Then incorporating with the Paris' law, the surface crack growth rate along the depth direction and length direction are predicted by

$$da/dN = C \cdot (\Delta K_{Ia})^m, \quad (2)$$

$$dc/dN = C \cdot (\Delta K_{Ic})^m, \quad (3)$$

where da/dN and dc/dN are the crack growth rate along the depth and length direction respectively (unit in mm/cycle). C and m are the Paris' constant. In this paper, we calibrate the values of C and m from the test results, as shown in Fig. 12.

Fig. 12 illustrated that the C for crack growth along the depth direction and the length direction are different, while the m is the same for crack growth along the two directions [27]. Therefore we use C_a and C_c as the constants for the depth and length direction respectively, where C_a equals to 5.424×10^{-16} and C_c equals to 4.143×10^{-16} . The m equals to 3.9 for both directions. Note that the unit for SIF in this paper is $\text{MPa} \cdot \text{mm}^{1/2}$.

3.4.2. Experimental validation

In this sub-section, the FE models are validated by the experimental results of surface crack growth. Take 'SE-1-R(1)' as an example, 'S'

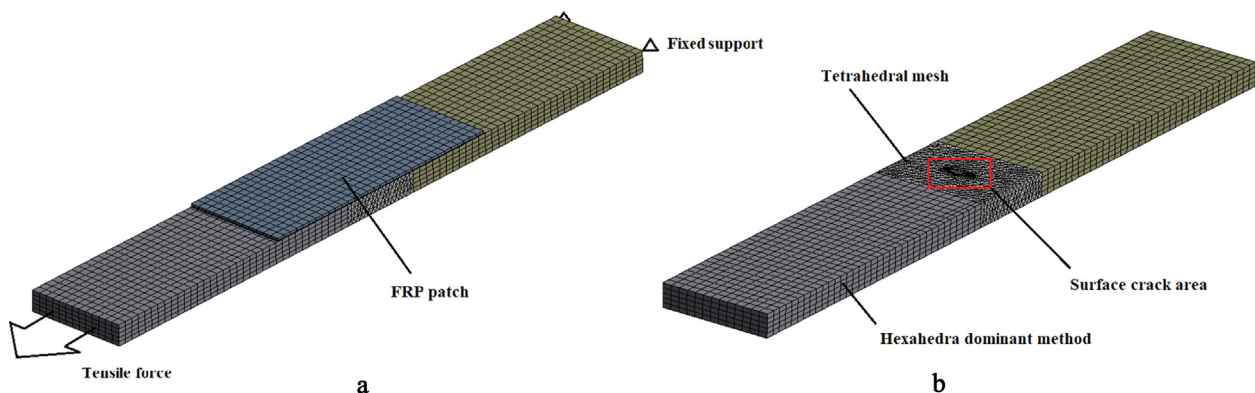


Fig. 6. FE model: a) global meshing condition and boundary condition; b) the surface cracked area and different meshing methods.

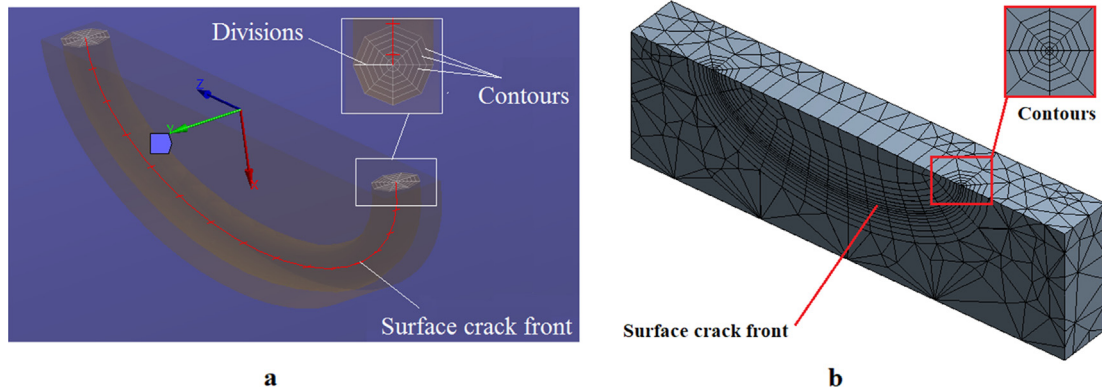


Fig. 7. a) Surface crack modelling module; b) the mesh around the surface crack.

means steel plate, ‘E’ represents reinforcing the steel plate on the cracked surface, ‘R’ means reinforcement, the first ‘1’ stands for the first type of notch, and the second ‘1’ means the No. of the repetitive specimen.

The SIF of the surface crack in the steel plate reinforced with FRP is calculated by means of the FE method. The procedure of evaluating the surface crack growth along the depth direction and length direction is indicated by Fig. 13. ΔK_{Ia} and ΔK_{Ib} are the SIF range of the deepest point and the surface point of the crack. Then the crack growth rate is evaluated by using the Paris’ law. Afterwards, by assuming a small amount of cycles, the increments of the crack length and depth are calculated. Eventually, it is possible to trace the surface crack growth along the two directions. The results of surface crack growth evaluated by the FE model and the Paris’s law are compared with the experimental results. Hence, the FE model of evaluating the SIF is validated by the experimental results.

The comparison between the FE results and the experimental results of surface crack growth of three different specimens categories are shown from Figs. 14 to 16. The figures indicate that the FE results match well with the experimental results when using FRP to reinforce the cracked surface of the steel plates, which means that the FE model can accurately evaluate the SIF of surface cracks reinforced with the sing-side FRP patch. In addition, the results indicate that FRP reinforcement has significantly decreased the surface crack growth and prolonged the fatigue life of specimens.

In addition to the validation of the SIF evaluation, the FE results of the strain data at the central of the external CFRP laminate are compared with the experimental results, in order to further validate the mechanical transmission within the FE model. The strain on the central point along the force direction of the specimen of ‘SE-1-R(2)’ under the

maximum load of 167.48 kN is 1058.18 $\mu\epsilon$, and the FE result is 1024 $\mu\epsilon$, with around 3.23% errors. It indicate that the FE result of strain at the central point on the external CFRP laminate agrees well with the experimental results, which means the FE model has rationally evaluated the mechanical transmission from the steel substrate through each FRP laminates to the external layer of the CFRP laminate.

4. Parametric study

In previous studies, researchers investigated the influential parameters on through-thickness crack growth in FRP reinforced steel plates [13]. However, their effects on surface cracked steel plates are unclear. In this regard, the parametric study is conducted by means of the FE model, and their effects has been quantitatively analysed.

4.1. Different reinforcement schemes

In this sub-section, three different reinforcement schemes, i.e., single-side FRP reinforcement on the cracked surface of the specimens or on the reversed side, and the double-side FRP reinforcement, are analysed and discussed. Note that four layers of CFRP laminates are applied for all single-side FRP reinforced specimens, while four layers of CFRP laminates are applied on both of the surfaces when using the double-side FRP reinforcement.

4.1.1. Single-side reinforcement on the reverse surface

Using the FRP to reinforce the cracked surface of a metallic structure may not be always feasible. In such situation, alternative reinforcement methods, such as reinforcing the reversed side of the cracked surface, might be an option. Therefore in this sub-section, we

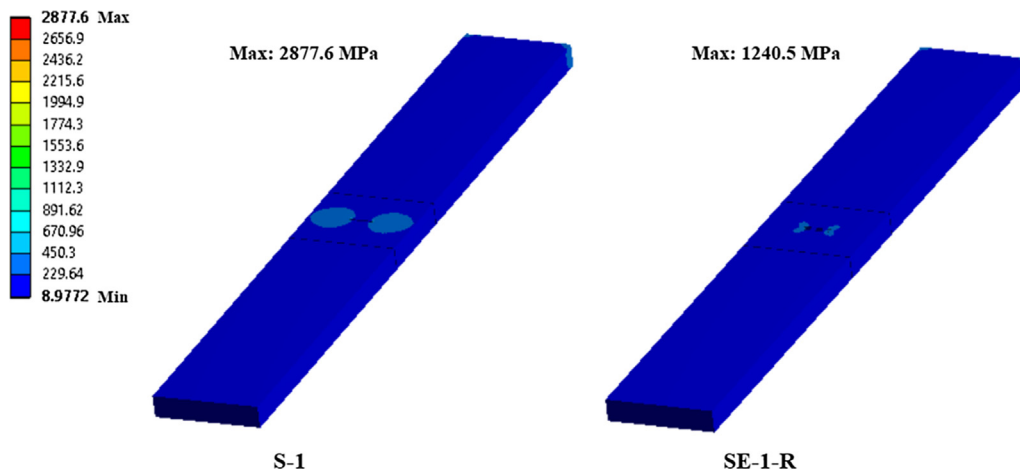


Fig. 8. The global equivalent stress distribution (von Mises) of the plate including the un-reinforced plate and the FRP reinforced specimen.

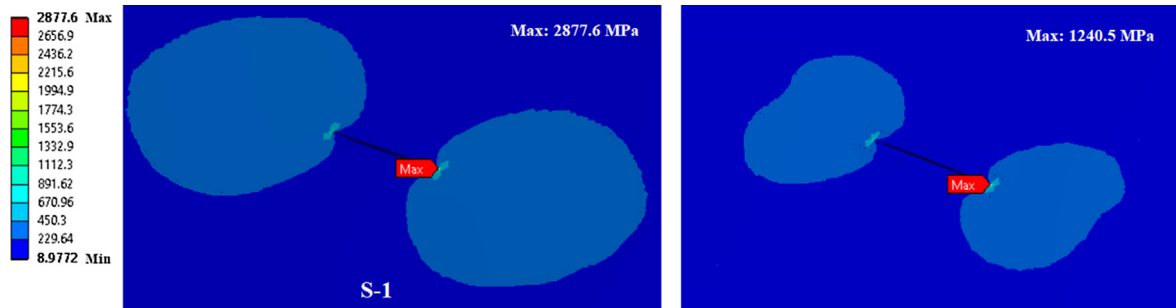


Fig. 9. The equivalent stress distribution (von Mises) around the surface crack on the cracked surface.

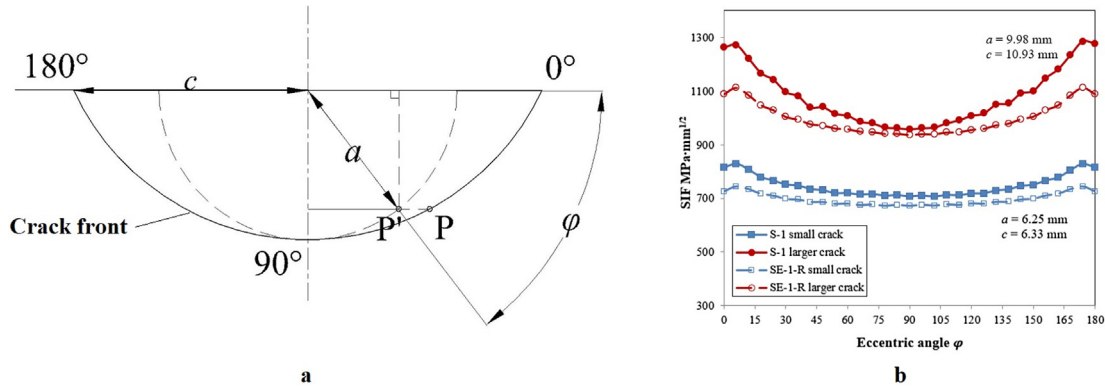


Fig. 10. The SIF distributions along the crack front: a) configuration of the surface crack; b) SIF along the crack front of different crack size.

discuss the effectiveness of single-side FRP reinforcement on the reverse side on the surface crack growth rate and the prolongation of fatigue life. The FE model is built on accordance with the test specimens. Then the FE results, as well as the comparison with the experimental results, are shown in Fig. 17.

As a result, the FRP reinforcement slightly increases the FCGR rather than decreasing the FCGR, owing to the out-of-plane bending moment on the steel plate generated by the asymmetric reinforcing

geometry, as indicated in Fig. 18. Fig. 18a illustrates that the FRP reinforcement has caused a bending deformation on the steel specimen where the surface crack located (when $a = 5.66$ mm, and $c = 6.54$ mm). Therefore, the stress distribution around the cracked area reinforced with FRP, of which especially closing to the cracked surface, is higher than the non-reinforced steel plates (228.3 MPa), as indicated in Fig. 18b. The higher stress concentration eventually results in higher SIF along the crack front.

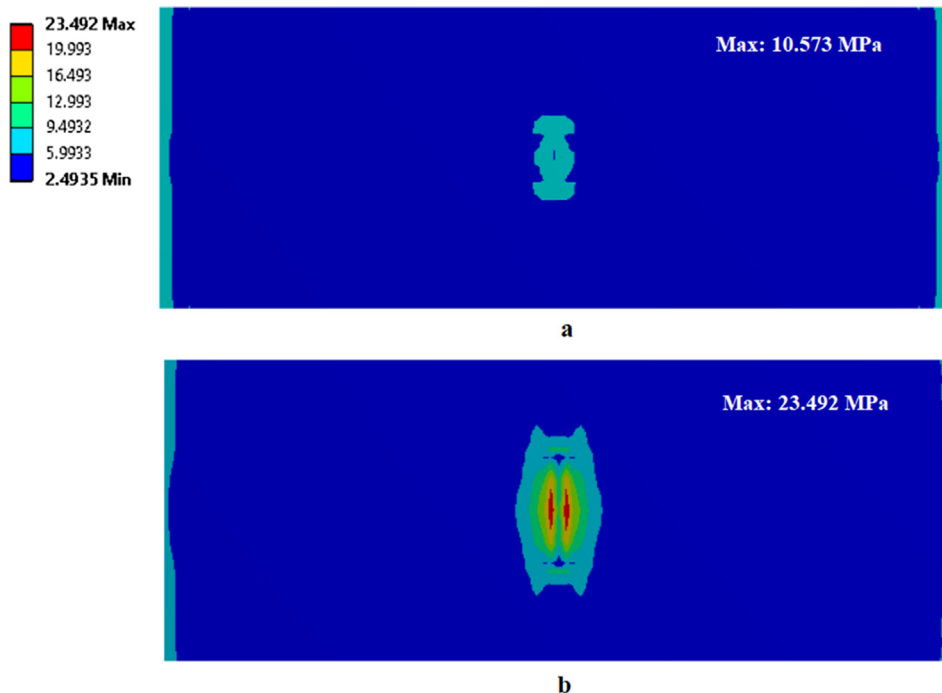


Fig. 11. The equivalent stress distribution (von Mises) of the adhesive layer: a) small crack; b) large crack.

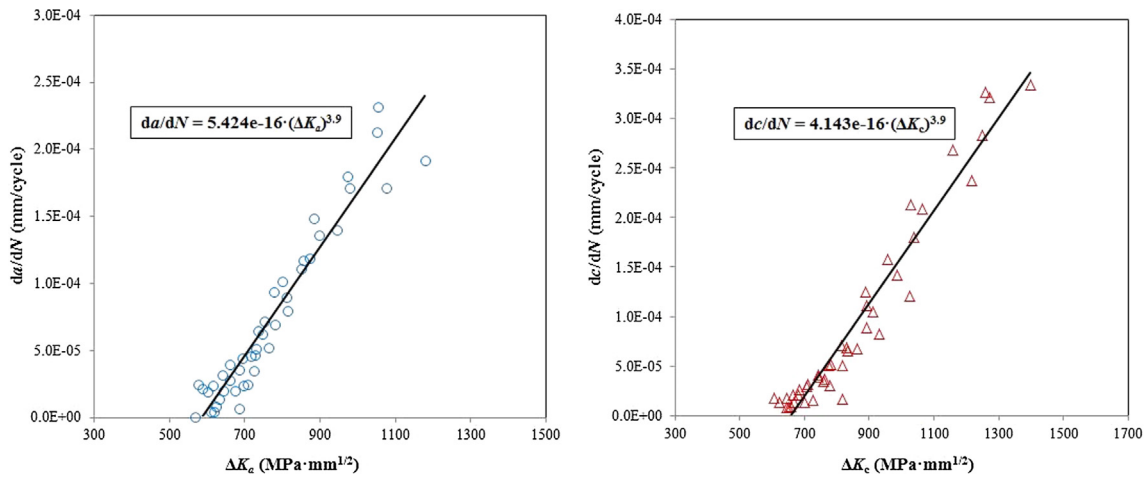


Fig. 12. Evaluation of the Paris' constants (C and m) from da/dN versus ΔK_{Ia} , and dc/dN versus ΔK_{Ic} .

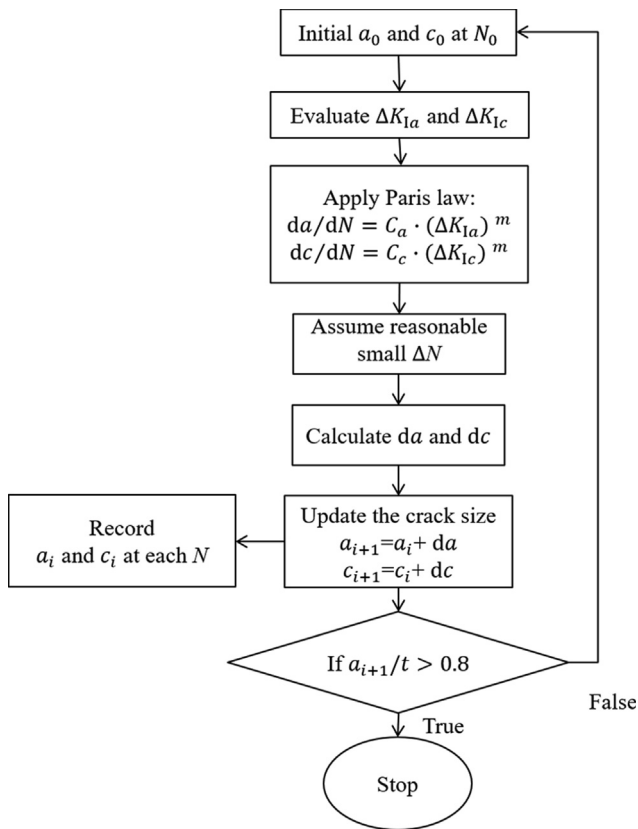


Fig. 13. The procedure of evaluating surface crack growth.

Fig. 18b also explains the SIF results shown in Fig. 10 when using the FRP to reinforce the surface cracks with different crack sizes. When the surface crack grows deeper, the stress concentration around the deepest point increases correspondingly due to the bending stress. Thus the reinforcement on the deeper crack does not performed as efficient as on the crack with a smaller crack depth. In addition, since the FRP reinforcement is invariably efficient on the cracked surface around the surface point, the SIF decreasing on the surface point is more significant than on the deepest point, regardless of the crack size.

4.1.2. Double-side reinforcement on both surfaces

Double-side reinforcement is more efficient on reinforcing the through-thickness cracked steel plates [28]. While its applicability on surface cracked plate remains unknown. In this part, we compared the

double-side reinforcement with the single-side reinforcement by means of the FEA. We choose the FE model of SE-2-R as the single-side reinforcement which applies one layer of GFRP and four layers of CFRP laminate on the cracked surface. While the double-side reinforcement applies one layer of GFRP and four layers of CFRP laminate on both sides, named as SE-2-RD. The FE results and their comparison are shown in Fig. 19.

Interestingly, the SE-2-RD which applies more FRP laminates performs less effectiveness than the single-side reinforcement on prolonging the fatigue life, especially on the crack growth along the length direction (see in Fig. 19b), results in a smaller preferred aspect ratio (a/c when $a/t = 0.8$), as illustrated by Fig. 19c. The reason of single-side reinforcement performing the best can be explained by the out-of-bending bending (see in Fig. 18) as well. In contrast with reinforcing the reversed side, the bending stress in this case facilitate the stress decreasing around the surface crack. However, the out-of-plane bending effect on the surface crack growth has been eliminated by the double-side FRP reinforcement, resulting in a less efficient performance on decreasing the surface crack growth.

Fig. 20 further shows the effect of FRP reinforcement on the SIF along the surface crack with two different sizes of either using the single-side FRP reinforcement on the cracked surface or double-side FRP reinforcement on both surfaces. The SIFs along the surface crack front under the single-side reinforcement are slightly smaller than those SIFs under the double-side reinforcement with a smaller crack (when $a = 4.48$ mm, $c = 4.68$ mm). While for the large crack (when $a = 10.23$ mm, $c = 11.33$ mm), the double-side FRP reinforcement performs slightly better than the single-side reinforcement on the deepest point but it performs worse on the surface point. Hence, since the crack growth is an accumulate process, the slower FCGR owing to the single-side reinforcement on a smaller crack finally facilitate the prolongation of the fatigue life.

The comparison of the stress distribution in the adhesive layer using the single-side FRP reinforcement and the double-side FRP reinforcement (when $a = 10.23$ mm, $c = 11.33$ mm) is shown in Fig. 21. Fig. 21a indicates that the stress using the double-side FRP reinforcement is basically identical but slight higher than using the single-side FRP reinforcement, owing to the fact that there is no bending effect on the double-side reinforced steel plate. In addition, owing to the out-of-plane bending effect, the stress value on the steel surface adjacent to the FRP reinforcement of using single-side reinforcement is smaller than using the double-side reinforcement. While the stress value gradually increases along the thickness direction and at around $t = 4$ mm, the stress value surpass the double-side reinforcement. In general, as shown in Fig. 19, the single-side reinforcement performs slightly better on decreasing the FCGR. The reasons might be that the stress distribution

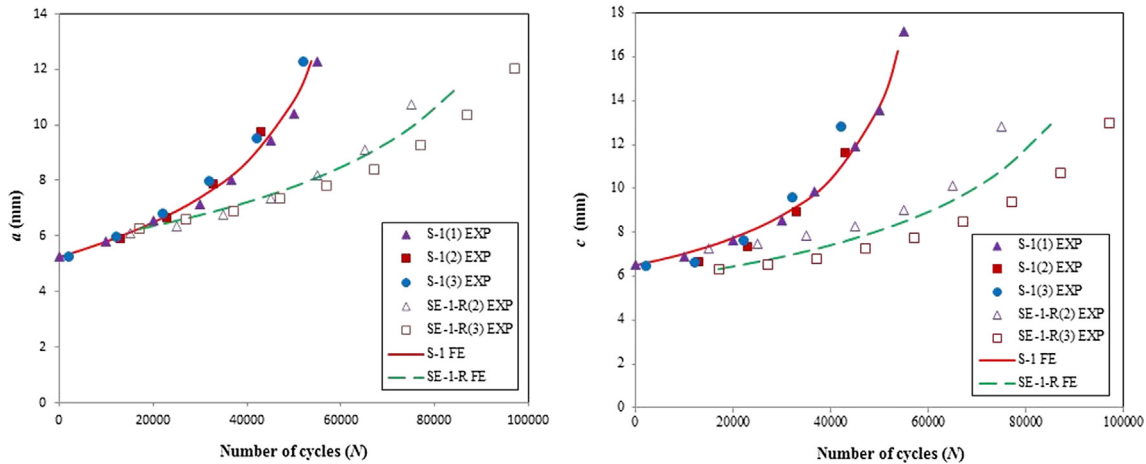


Fig. 14. The comparison of FE results and experimental results on S-1 and SE-1-R specimens.

is always smaller around the surface point, which reduces the crack growth along the length direction, which reduces the crack growth along the depth direction to some extent as well.

In summary, among the three reinforcement method, the single-side FRP reinforcement on the cracked surface performs the best on decreasing the FCGR of the surface cracks. The double-side FRP reinforcement performs well on decreasing the FCGR, while there is no obvious advantage over the single-side FRP reinforcement such as decreasing the stress distribution in the adhesive layer. Hence in light of the doubled cost and reinforcement time, the double-side FRP reinforcement is not suggested in practical situations.

4.2. Bond length of the FRP patch

The bond length is one of the easiest parameters to be changed in practice which could affect the budget and time-consuming of the project. In addition, it might significantly influence the reinforcement effectiveness. The main purpose of this section is to find a sound and cost-effective bond length for practical usage. In this study, we investigated the bond length ranging from 30 mm to 200 mm.

From this sub-section to Section 4.7, the SIFs along the crack front of different models are calculated based on the crack size of $a = 5.33$ mm, $c = 5.90$ mm, which is the starting size of FE model ‘SE-1-R’. The SIF reduction results of the FE models by applying different bond lengths, compared to the unreinforced FE model, is shown in Fig. 22. It clearly shows there exists a sufficient bond length, which is 80 mm. The bond length of 30 mm only has a minor effect on the reduction of the SIF.

Increasing the bond length can further decrease the SIF of the surface crack, while the added effect becomes less and less significant until the bond length reaches 80 mm. Then the SIF reduction proportion remains stable within the increase of the bond length.

4.3. Numbers of bond layer

Applying more layers of CFRP laminates is another practical approach that might affect the reinforcement effectiveness, since the study on FRP reinforced through-thickness cracked steel plates subjected to tension has indicated its efficiency [15]. In this sub-section, the influence on surface crack growth is investigated, by applying six different numbers of CFRP layer, ranging from one to six. Note that the one layer of GFRP is always applied as the first layer in between the steel substrate and the CFRP laminates. In addition, the bond length of 150 mm is chosen for all FE models in the following sub-sections.

Fig. 23 shows that similar to the bond length, increasing the numbers of bond layer does not always decrease the SIF of the surface crack. In fact, there exist an optimum number of bond layers on the 12.3 mm thickness steel plate – two layers of CFRP laminates (0.7 mm), while beyond that, the effectiveness of the FRP reinforcement start to reduce. The FE results are agreed well with the experimental results, as shown in Fig. 24, by simulating the surface crack growth reinforced with two layers or four layers of CFRP laminates respectively. In addition, there only has a minor difference of the results between using two layers of CFRP and four layers of CFRP laminates.

As is indicated in Fig. 24, two layers of CFRP laminate is the

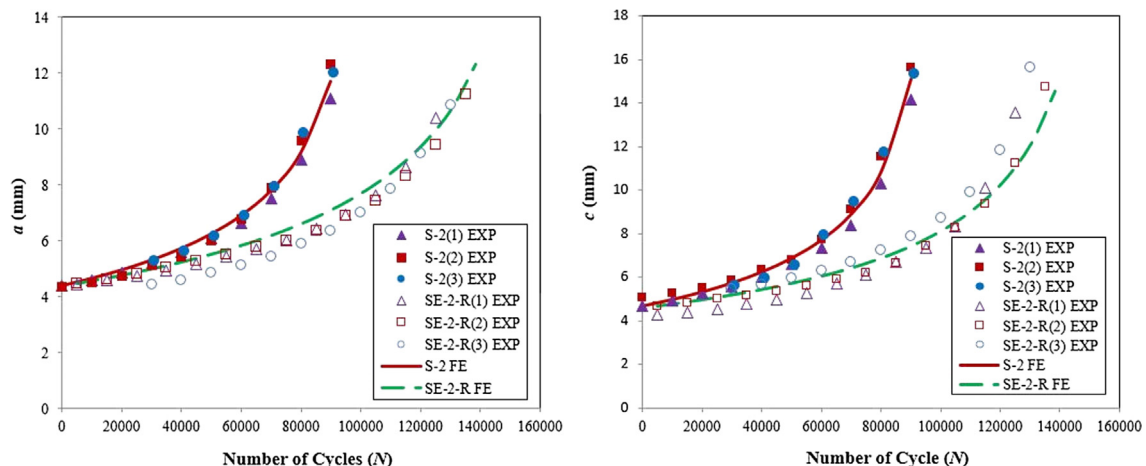


Fig. 15. The comparison of FE results and experimental results on S-2 and SE-2-R specimens.

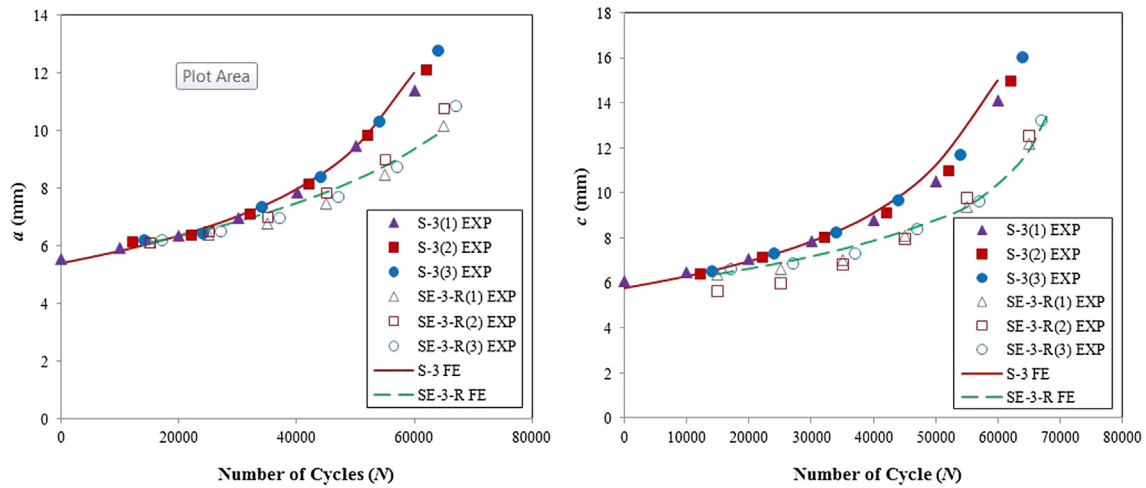


Fig. 16. The comparison of FE results and experimental results on S-3 and SE-3-R specimens.

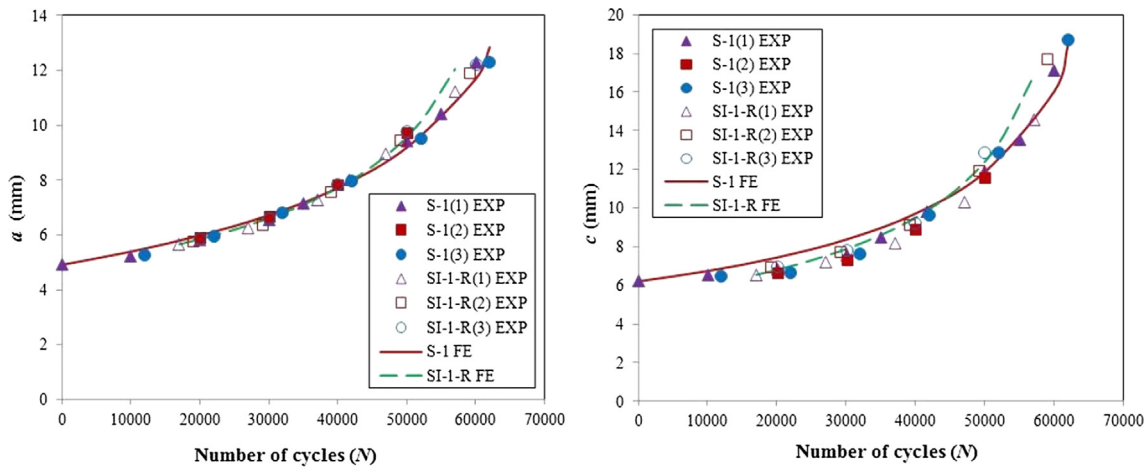


Fig. 17. The comparison of FE results and experimental results on S-1 and SI-1-R specimens.

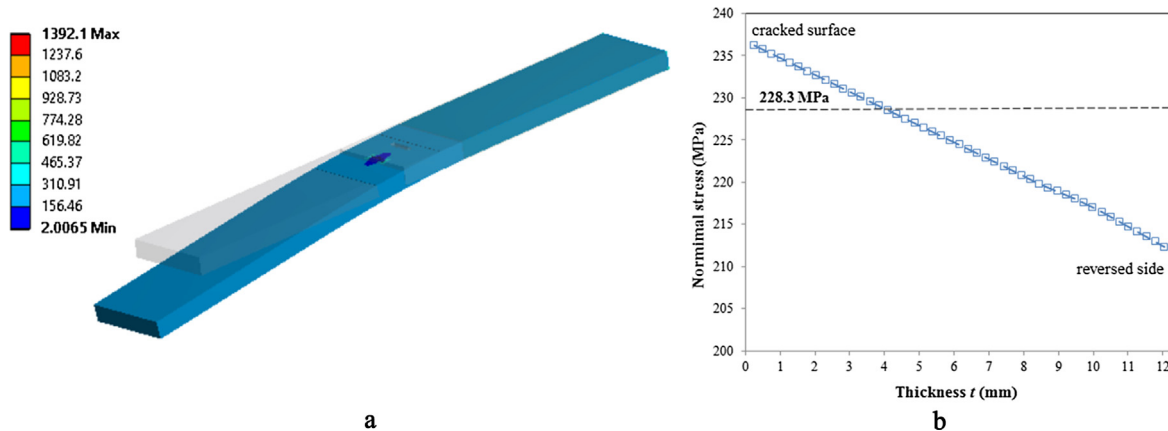


Fig. 18. Stress distribution of the SI-1-R model: a) global stress distribution (von Mises) and deformation (90 times of the true scale); b) normal stress distribution of the path in the centre along the wall-thickness direction (exclude the surface crack).

optimum for the plate whose thickness equals to 12.3 mm, while whether it is the optimum for different thickness steel plates is uncertain. Given that, we conducted the sensitivity study on steel plates with thickness from 8 mm to 16 mm with 2 mm interval. The results of the SIF reduction of the surface point are shown in Fig. 25, surprisingly indicating that two layers of CFRP laminate is the optimum for all different thickness steel plates. The reason is that the optimum bond

layer (bond thickness) shares the maximum displacement and stress from the tensile steel plate. While applying more layers of CFRP laminates would not promote for the effect on the SIF reduction.

4.4. CFRP tensile modulus

The rapid development of material technology has led an increasing

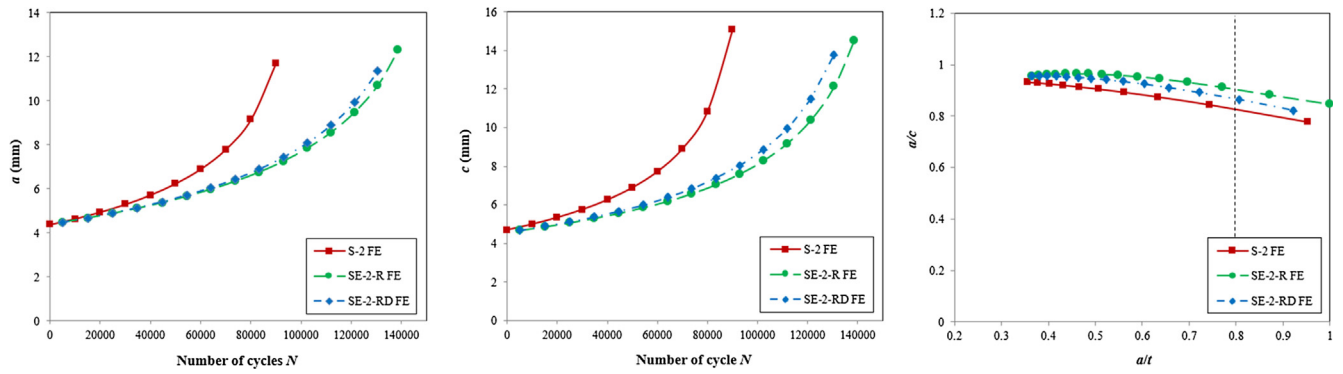


Fig. 19. The comparison of FE results on SE-2-R and SD-2-R models.

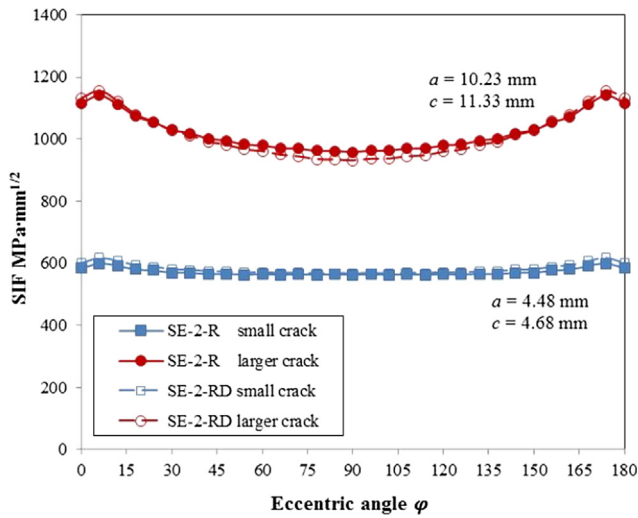


Fig. 20. FE results comparison of SIF along the surface crack between using single-side reinforcement on the cracked surface and the double-side reinforcement.

on the material properties of the CFRP laminates. The tensile modulus is one of its most important property. At present, there are a variety of CFRP materials in the global market. In this sub-section, we study three representative CFRP materials with the tensile modulus of 150, 230, and 552 GPa respectively. For all FE models, the SIF is transformed into

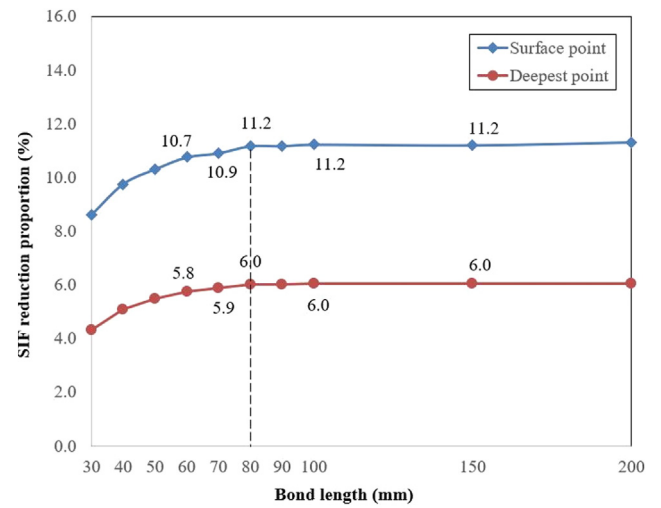


Fig. 22. The SIF reduction results of the deepest point and the surface point with different bond length.

the normalised SIF K_{nor} to better illustrate the effect of the influential parameters on the SIF, which is the quotient of the SIF along the crack front K and the SIF of the deepest point of the surface crack K_{Ic} (the largest SIF for this crack), calculated as $K_{nor} = K/K_{Ic}$.

It is surprising to see that the tensile modulus of CFRP laminate has a minor influence on the SIF reduction of the surface crack, as indicated

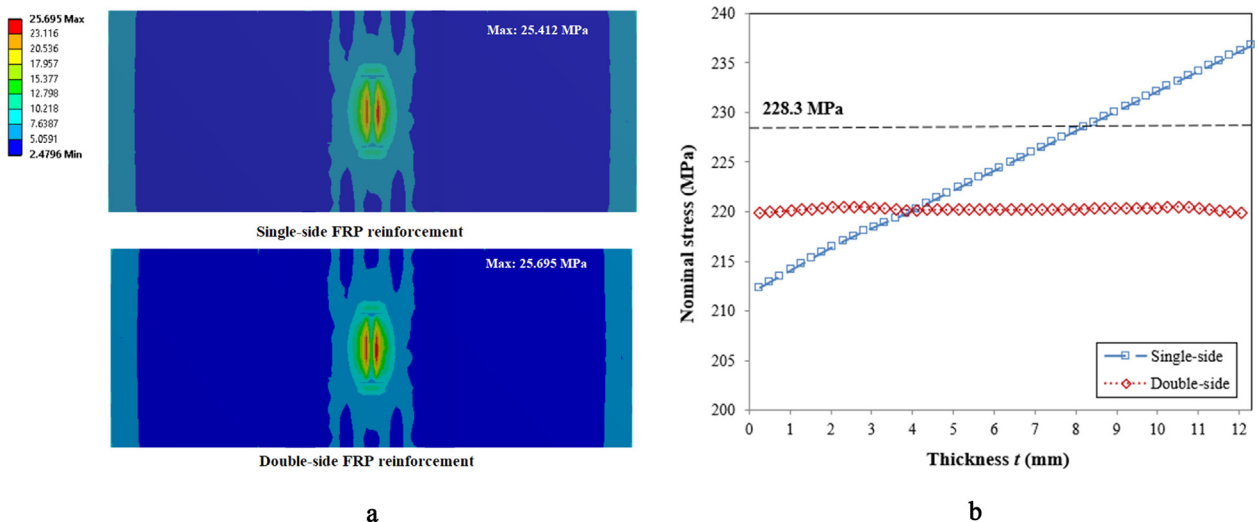


Fig. 21. The comparison between the single-side and double-side reinforcement on stress distribution: a) stress concentration (von Mises) in the adhesive layer; b) nominal stress distribution of the path in the centre along the wall-thickness direction (exclude the surface crack).

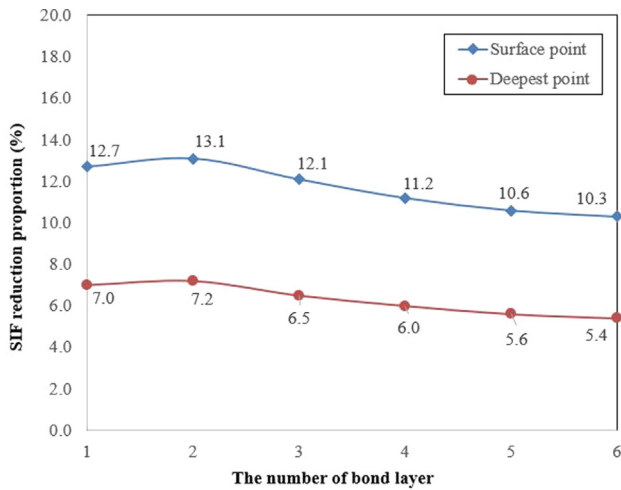


Fig. 23. The SIF reduction results of the deepest point and the surface point with different number of bond layer.

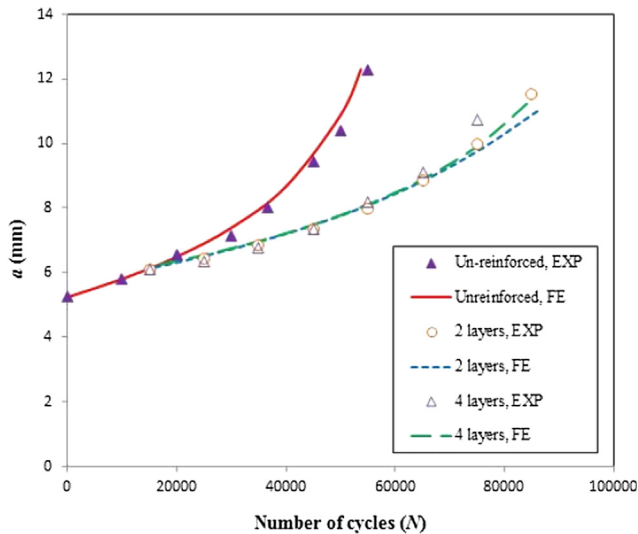


Fig. 24. The FE and experimental results of the cracked plate by using two layers and four layer of CFRP respectively.

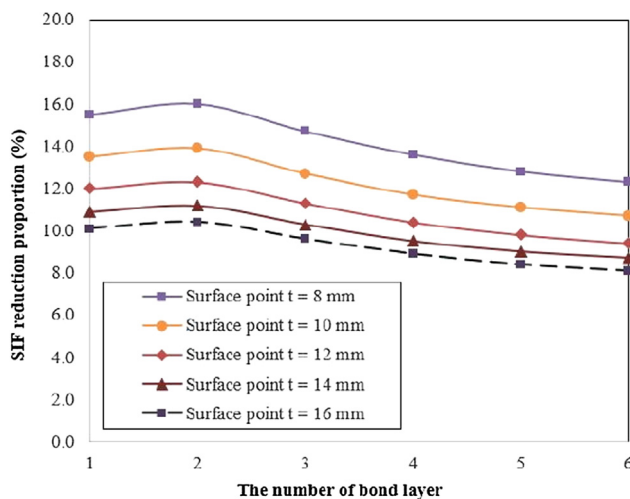


Fig. 25. The SIF reduction results of the surface point on steel plates with different thickness by using different numbers of bond layer.

in Fig. 26a. Note the SIF values has been normalised to better illustrate the effect on the SIF, which is the quotient of the SIF along the crack front and the SIF of the deepest point of the surface crack (the largest SIF along the crack front). Fig. 26b further illustrated that by showing the SIF reduction proportion. The CFRP with the tensile modulus of 230 GPa indeed performs better than the CFRP with the tensile modulus of 150 GPa, while the improvement of the effectiveness by further increasing the tensile modulus becomes negligible. Therefore in practical situations, choosing CFRP material with high tensile modulus is not suggested from the economic perspective.

4.5. Adhesive thickness

The adhesive layer is the intermediary between the steel substrate and the FRP laminates, which is the weakest layer in the reinforcement system. In this sub-section therefore, both the reinforcement effectiveness and the stress distribution in the adhesive layer by using different adhesive thicknesses are investigated. Five ranges of the adhesive thickness from 0.1 to 0.5 mm are adopted.

Fig. 27 shows that increasing the adhesive thickness insignificantly contributes to the SIF reduction. However, the stress distributed in the adhesive layer is very sensitive to the thickness of the adhesive, especially when increasing the adhesive thickness from 0.1 mm to 0.3 mm, as indicated in Fig. 28. For all FE models, the maximum stress occurs around the cracked area. Although the stress slightly decreased with the adhesive thickness of 0.5 mm, overall speaking, the maximum stress increases within the increasing of the adhesive thickness. Thus in this case, the adhesive thickness needed to be controlled as a relatively thin level in order to avoid adhesion failure.

4.6. Crack aspect ratio

Since the causes of surface cracks in steel structures are various, the aspect ratio of surface crack can be diverse as well. In this section, the SIF reduction response to the crack aspect ratio is analysed. Six sets of surface cracks with different aspect ratio, ranging from 0.25 to 2.0 have been arranged. Table 6 shows the detailed crack sizes of each FE model, as well as the SIF reduction results of the deepest point and the surface point respectively.

Clearly, Table 6 illustrates that within the increase of the crack aspect ratio, the SIF reduction of the deepest point is decreasing, while the SIF reduction of the surface point is insensitive to the crack aspect ratio. In light of Model No. 4 to No. 6 which has the same crack depth, the SIF reduction proportion reduces from 4.9% to 3.2% of the deepest point. These results in Table 6 indicate that FRP reinforcement is more efficient on reducing the SIF on the deepest point of surface cracks with a small aspect ratio.

4.7. Crack dimensions

Section 4.6 indicates that FRP reinforcement preforms better on the surface crack with small aspect ratio, but in fact, the aspect ratio is changing constantly during the fatigue process. Therefore, in this subsection, we investigate the effectiveness of the FRP reinforcement on the SIF reduction during the fatigue cracking process. The FE model SE-1-R is adopted, starting from the crack size of $a = 5.33$ mm, and $c = 5.90$ mm till $a = 9.98$ mm, and $c = 10.93$ mm. The crack depths were selected from the FE results of SE-1-R, thus we developed the FE models with the selected crack sizes during the cracking process. Then the SIF of the surface crack (surface point and deepest point) with different crack sizes were evaluated.

As shown in Fig. 29, it is interesting to see that the trends of the surface point and the deepest point along with the crack growing process are diverse – the SIF reduction of the surface point becomes more significant, whereas the SIF reduction on the deepest point becomes insignificant. The reason for the decreasing of the SIF reduction

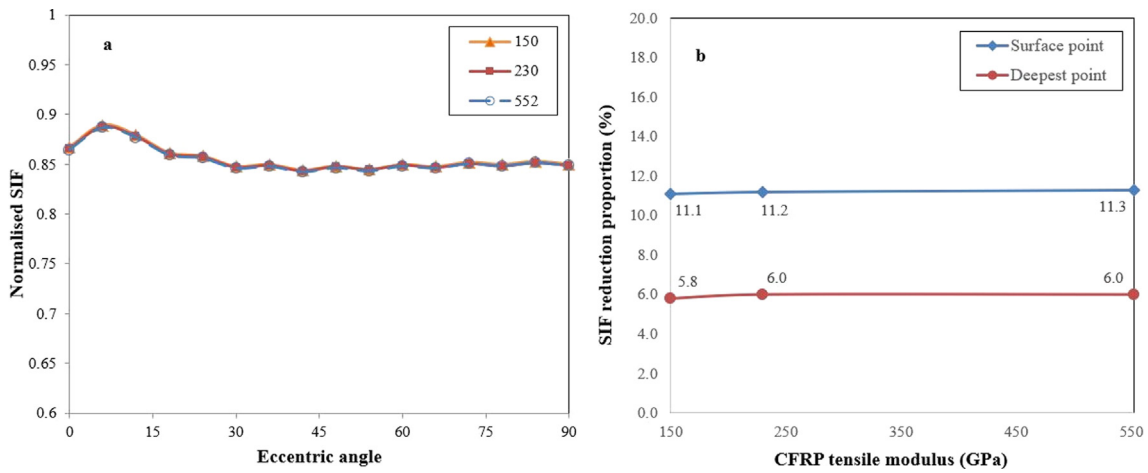


Fig. 26. The SIF response of the FE models with different CFRP tensile modulus: a) the normalised SIF result along the crack front; b) the SIF reduction proportion of the deepest point and the surface point.

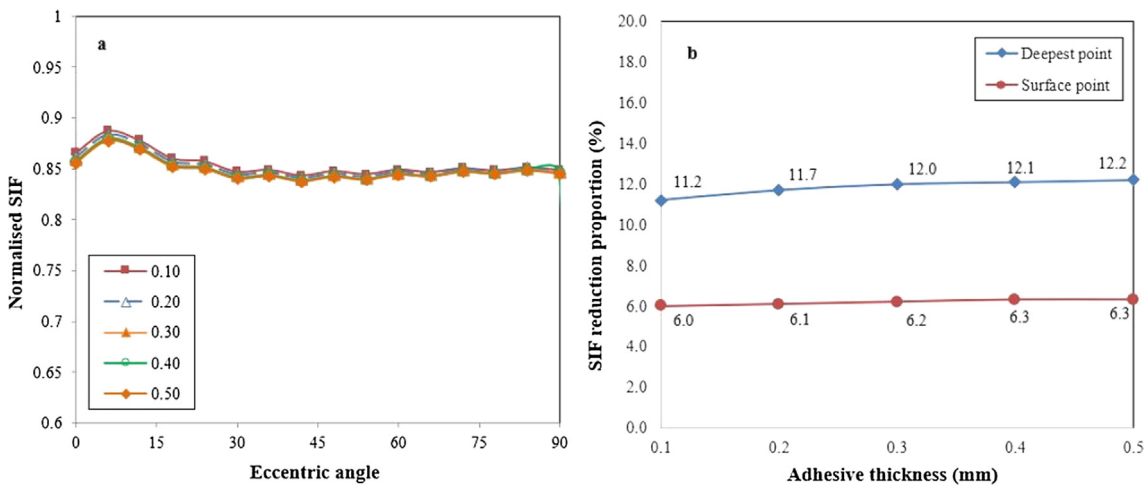


Fig. 27. The SIF response of the FE models with different adhesive thickness: a) the normalised SIF result along the crack front; b) the SIF reduction proportion of the deepest point and the surface point.

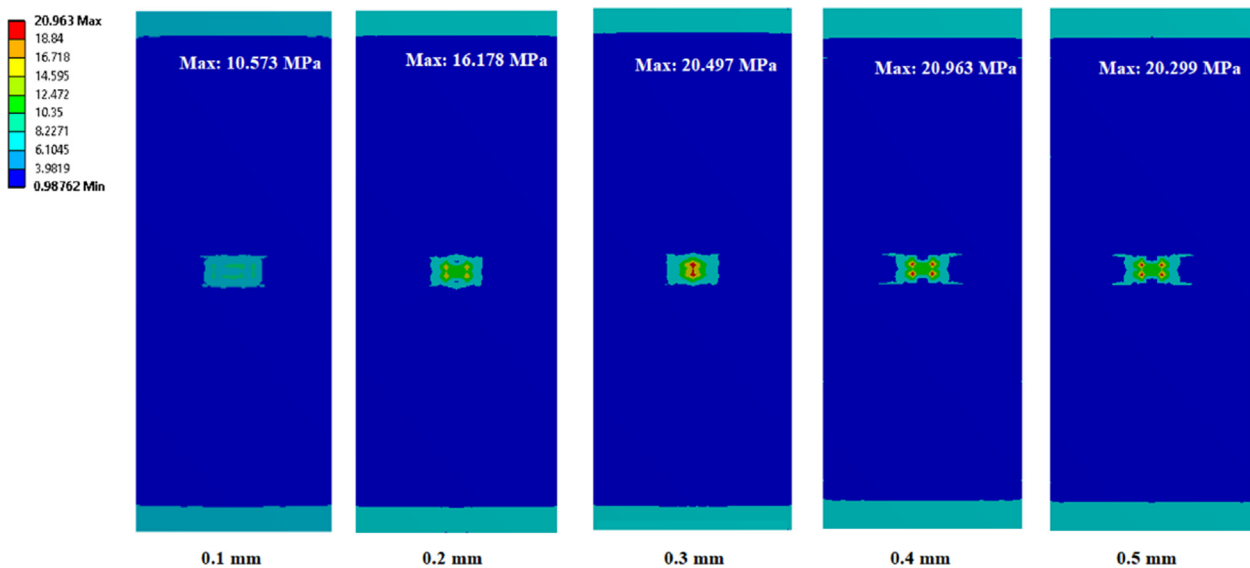


Fig. 28. The stress distribution (von Mises) in the adhesive layer with different thickness.

Table 6
Specimen configuration of steel plates with different aspect ratios.

| Model No. | a (mm) | c (mm) | a/c | SIF reduction of the deepest point | SIF reduction of the surface point |
|-----------|--------|--------|------|------------------------------------|------------------------------------|
| 1 | 3.0 | 12.0 | 0.25 | 8.8% | 10.6% |
| 2 | 3.0 | 6.0 | 0.5 | 7.3% | 9.9% |
| 3 | 4.5 | 6.0 | 0.75 | 6.2% | 10.3% |
| 4 | 6.0 | 6.0 | 1.0 | 4.9% | 10.3% |
| 5 | 6.0 | 4.5 | 1.5 | 3.9% | 9.7% |
| 6 | 6.0 | 3.0 | 2.0 | 3.2% | 9.2% |

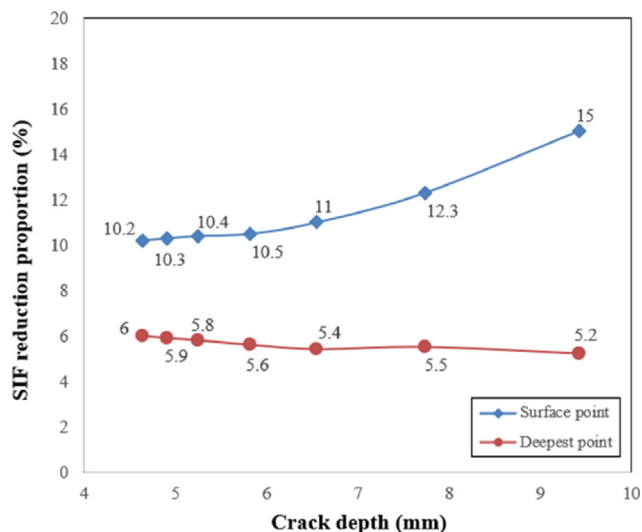


Fig. 29. The SIF reduction results of the deepest point and the surface point with different crack dimensions along with the crack growing process.

proportion on the deepest point is owing to the out-of-plane bending moment that when the crack grows deeper, the stress around the deepest direction becomes higher. While the reason for the increasing of the SIF reduction proportion on the surface point is owing to the decreasing of the stress around the surface point along with the increasing of the crack length. Therefore, in consideration of that preventing surface crack growth from penetrating the wall thickness is of great importance, reinforcing the surface crack as early as possible is suggested, in order to achieve the optimum fatigue life extension.

5. Conclusions

In this paper, we investigate the surface crack growth in FRP reinforced steel plates subjected to tension by means of the FE method. The FE model is first developed and validated by the experimental investigation. Then based on the validated FE model, a parameter study has been conducted to identify the optimum reinforcement schemes and the key influential parameters of the FRP reinforcement. The conclusions can be drawn:

- The FE method is able to accurately evaluate the SIF along the surface crack in the FRP reinforced steel plate subjected to tension. The FE results, as well as the experimental results indicate that single-side FRP reinforcement on the cracked surface can significantly decrease the FCGR and prolong the residual fatigue life. For instance, the FE results show that single-side FRP reinforcement on the cracked surface has prolonged the residual fatigue life of FE model ‘S-2’ which penetrated the wall thickness of 35.6% of approximately 52.63%.
- The single-side FRP reinforcement performs better on the crack growth along the length direction than along the depth direction,

owing to the crack-bridging effect, as well as the effect of the out-of-plane bending moment. This results in the increasing of the preferred aspect ratio of the FRP reinforced surface cracks.

- The parametric study indicates that among the three reinforcement method, single-side FRP reinforcement on the cracked surface performs the best on decreasing the FCGR and prolonging the fatigue life. The double-side reinforcement performs slightly less effective with doubled cost and time. Nevertheless, only reinforcing the reversed side of the cracked surface is not an appropriate reinforcement method, because the stress distribution around the surface crack has been increased by the out-of-plane bending moment.
- The parametric study also indicates that there exist an optimum bond length and numbers of bond layer. While the SIF is less sensitive to influential parameters such as the CFRP tensile modulus, and adhesive thickness. In practical situations, overall considering the effects on the SIF and the stress concentration in the adhesive layer, as well as the reinforcement cost and time, two layers of normal tensile modulus CFRP laminates with the bond length of at least 80 mm are suggested, and the adhesive layer is needed to be controlled as a relatively thin level. Besides, the parametric study indicates the FRP reinforcement is more efficient on reducing the SIF of surface cracks with a small aspect ratio. Along with the crack growing process, the FRP reinforcement becomes more effect on decreasing the SIF of the surface point, while less efficient on the deepest point. Therefore, it is suggested to reinforce the surface crack as early as possible, in order to achieve the optimum fatigue life extension before the crack penetrating the wall thickness.

This study conducting on the surface crack plate under tension, is the fundamental research for our research on using composite materials to reinforce surface cracked metallic pipes. It is of significant value in terms of understanding the reinforcing mechanism, and identifying the FE method. The reinforcement methods and influential parameters within this study have a guiding significance towards FRP reinforcement on surface cracked structures. However, influential factors such as fibre orientation were not considered. Such investigations will be presented in our future studies.

CRedit authorship contribution statement

Zongchen Li: Conceptualization, Methodology, Validation, Formal analysis, Data curation, Writing - original draft, Writing - review & editing, Visualization. **Xiaoli Jiang:** Conceptualization, Writing - review & editing, Supervision. **Hans Hopman:** Supervision, Funding acquisition. **Ling Zhu:** Resources, Funding acquisition. **Zhiping Liu:** Resources, Funding acquisition.

Declaration of Competing Interest

The authors declare that they have no known competing financial interests or personal relationships that could have appeared to influence the work reported in this paper.

Acknowledgement

The authors appreciate Department of Maritime and Transport Technology, Delft University of Technology, the Netherlands for sponsoring this research. The experimental investigation was supported by Overseas Expertise Introduction Project for Discipline Innovation - 111 project of Chinese Ministry of Education and State Administration of Foreign Experts Affair of P. R. China [grant number 444110356] and Department of Maritime and Transport Technology, Delft University of Technology, the Netherlands. The Key Laboratory of High Performance Ship Structure of the Chinese Ministry of Education is also appreciated for providing the experimental facilities. The first author would like to

acknowledge the China Scholarship Council, P. R. China [grant number 201606950024] for funding his research.

References

- [1] J. Schijve, *Fatigue of Structures and Materials*, Springer Science & Business Media, 2001.
- [2] H.A. Richard, M. Sander, *Fatigue Crack Growth*, Springer, 2016.
- [3] Z. Li, X. Jiang, H. Hopman, Surface crack growth in offshore metallic pipes under cyclic loads: a literature review, *J. Mar. Sci. Eng.* 8 (5) (2020) 339.
- [4] J. Newman Jr, I. Raju, An empirical stress-intensity factor equation for the surface crack, *Eng. Fract. Mech.* 15 (1–2) (1981) 185–192.
- [5] L. Zhu, X. Tao, L. Cengdian, Fatigue strength and crack propagation life of in-service high pressure tubular reactor under residual stress, *Int. J. Press. Vessels Pip.* 75 (12) (1998) 871–877.
- [6] P. Singh, K. Vaze, V. Bhasin, H. Kushwaha, P. Gandhi, D.R. Murthy, Crack initiation and growth behaviour of circumferentially cracked pipes under cyclic and monotonic loading, *Int. J. Press. Vessels Pip.* 80 (9) (2003) 629–640.
- [7] Z. Li, X. Jiang, Z. Liu, H. Hopman, Internal Surface crack growth in offshore rigid pipes reinforced with CFRP, in: *ASME 2018 37th International Conference on Ocean, Offshore and Arctic Engineering*, American Society of Mechanical Engineers, 2018, pp. V004T03A022-V004T03A022.
- [8] Z. Li, X. Jiang, H. Hopman, Numerical analysis on the SIF of internal surface cracks in steel pipes reinforced with CRS subjected to bending, *Ships Offshore Struct.* (2019) 1.
- [9] Ž. Domazet, Comparison of fatigue crack retardation methods, *Eng. Fail. Anal.* 3 (2) (1996) 137–147.
- [10] X. Zhao, L. Zhang, State-of-the-art review on FRP strengthened steel structures, *Eng. Struct.* 29 (8) (2007) 1808–1823.
- [11] Z. Li, X. Jiang, G. Lodewijks, The latest development of reinforcement techniques on tubular joints, *Prog. Anal. Des. Marine Struct.* (2017) 783–790.
- [12] Z. Liu, K. Chen, Z. Li, X. Jiang, Crack monitoring method for an FRP-strengthened steel structure based on an antenna sensor, *Sensors* 17 (10) (2017) 2394.
- [13] Q. Yu, X. Zhao, Z. Xiao, T. Chen, X. Gu, Evaluation of stress intensity factor for CFRP bonded steel plates, *Adv. Struct. Eng.* 17 (12) (2014) 1729–1746.
- [14] Q. Yu, T. Chen, X. Gu, X. Zhao, Z. Xiao, Fatigue behaviour of CFRP strengthened steel plates with different degrees of damage, *Thin-Walled Structures* 69 (2013) 10–17.
- [15] H. Wang, G. Wu, Y. Pang, Theoretical and numerical study on stress intensity factors for FRP-strengthened steel plates with double-edged cracks, *Sensors* 18 (7) (2018) 2356.
- [16] P. Colombi, G. Fava, L. Sonzogni, Fatigue crack growth in CFRP-strengthened steel plates, *Compos. B Eng.* 72 (2015) 87–96.
- [17] J. Chen, H. Pan, Stress intensity factor of semi-elliptical surface crack in a cylinder with hoop wrapped composite layer, *Int. J. Press. Vessels Pip.* 110 (2013) 77–81.
- [18] Z. Li, X. Jiang, H. Hopman, L. Zhu, Z. Liu, An investigation on the circumferential surface crack growth in steel pipes subjected to fatigue bending, *Theor. Appl. Fract. Mech.* 105 (2020) 102403.
- [19] Z. Li, X. Jiang, H. Hopman, L. Zhu, Z. Liu, W. Tang, Experimental investigation on FRP-reinforced surface cracked steel plates subjected to cyclic tension, *Mech. Adv. Mater. Struct.* (2020) 1–15.
- [20] Specification for 907A prefiled of military ship (in Chinese), *GJB 6055-2007*, 2007.
- [21] E. ASTM, 2899, Standard Test Method for Measurement of Initiation Toughness in Surface Cracks Under Tension and Bending, vol. 3, 2015.
- [22] ASTM, ASTM E647. Standard Test Method for Measurement of Fatigue Crack Growth Rates, 1994.
- [23] B. Zheng, M. Dawood, Fatigue crack growth analysis of steel elements reinforced with shape memory alloy (SMA)/fiber reinforced polymer (FRP) composite patches, *Compos. Struct.* 164 (2017) 158–169.
- [24] S. Wang, I. Choi, Boundary-layer effects in composite laminates: part 1—free-edge stress singularities, 1982.
- [25] D. Leguillon, E. Sanchez-Palencia, *Computation of Singular Solutions in Elliptic Problems and Elasticity*, John Wiley & Sons Inc, 1987.
- [26] ANSYS, Semi-elliptical Crack. Defines a semi-elliptical crack based on an internally generated mesh to analyze crack fronts by use of geometric parameters. Available: https://ansyshelp.ansys.com/account/secured?returnurl=/Views/Secured/corp/v191/wb_sim/ds_Crack_o_r.html.
- [27] D.L. Corn, A study of cracking techniques for obtaining partial thickness cracks of pre-selected depths and shapes, *Eng. Fract. Mech.* 3 (1) (1971) 45–52.
- [28] H. Liu, R. Al-Mahaidi, X.-L. Zhao, Experimental study of fatigue crack growth behaviour in adhesively reinforced steel structures, *Compos. Struct.* 90 (1) (2009) 12–20.